 CMES, vol.72, no.2, pp.149-166, 2011

Numerical Modeling of Resin Film Infusion Process with Compaction and Its Application

Duning Li[1], Yufeng Nie[1,2], Xuemei Zhou[1] and Li Cai[1]

Abstract: In this study, the efficient discrete model including the resin infusion and the fiber compaction is developed to simulate the RFI (resin film infusion) process. The non-linear governing equations are derived by the Darcy's law, the Terzaghi's law and the continuity equations. The finite element method and the finite difference method are used to discretize the proposed equations, and the VOF method is used to track the filling front. Compared with the analytical results of Park, our numerical results agree well with them. Furthermore, we analyze the RFI process of BMI/G0814, and simulate the resin pressure, the fiber volume fraction distribution, the preform thickness et al to achieve the corresponding optimizing conditions. Some effects of parameters such as the resin thickness, the bleeder thickness, and the external pressure are also discussed here.

Keywords: C. Finite element analysis (FEA); E. Resin film infusion; E. Resin flow; E. Fabric compaction

1 Introduction

RFI process is one of the liquid composite molding (LCM) processes. It is a cost-effective process for the manufacture of large and complex-shaped composite structures. Unlike the resin transfer molding (RTM) process, the resin film is liquefied and absorbed transversely through the thickness of the fabric preform under the specific temperature and pressure conditions (Fig. 1). The resin should infiltrate the preform fully before the resin starts to gel. Otherwise, there will be unfilled region in the final part. Hence, it is of significance to simulate the resin flow in the fabric preform.

The basic flow phenomenon in the RFI process is similar to that in the RTM process, thus many researchers have employed the model used in the RTM process to

[1] School of Science, Northwestern Polytechnical University, Xi'an 710129, China
[2] Corresponding author, E-mail address: yfnie@nwpu.edu.cn

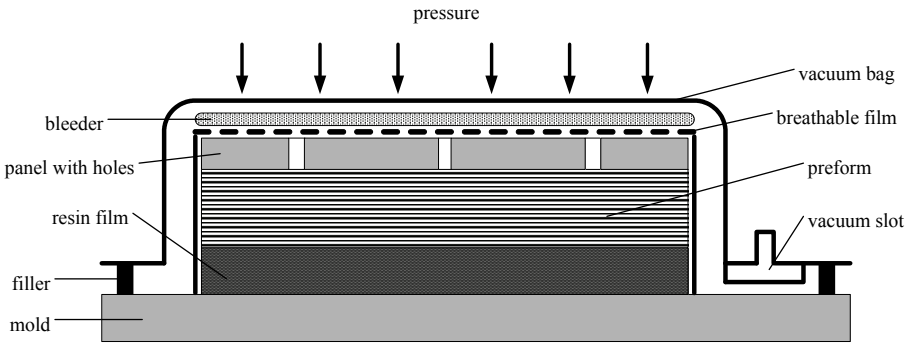

Figure 1: Schematic principle of RFI process.

simulate the RFI process. Loos et al. (1996) simulated the non-isothermal infiltration of a hot-melt resin into a single blade-stiffened panel. They proposed the Darcy flow models to describe the resin infiltration in a fibrous porous media, and used the finite element/control volume method for the simulation. Park et al. (2003) proposed a numerical analysis by considering the volume deformation of the fabric preform for the RFI process. But the fiber volume fraction distribution wasn't offered in that work. Han et al. (2003) simulated a non-isothermal RFI process for unstitched and stitched stiffened panels, and compared the performance of stitched stiffened panels with that of the unstitched stiffened panels. Celle et al. (2008) proposed an overall model for the study of a non-isothermal fluid flow across a highly compressible porous medium by using the ALE formulation.

To characterize the flow phenomenon, we must realize that the principal resin flow and the fabric compaction occur in the same direction during the RFI process. Thus, it's different from the flow phenomenon in other processes, such as VARI [Govignon et al. (2010)]; CRTM [Shojaei (2006)]. Ouahbi et al. (2007) developed a comprehensive numerical model for the hydro-mechanical coupling in infusion process. Park et al. (2009) proposed a one-dimensional model by taking into account the fabric preform compaction in the analysis of resin infusion processes, and the analytical solutions of resin infusion processes were presented.

After the resin has impregnated the preform fully in the RFI process, the fabric preform will keep on deforming under the external pressure. If the resin starts to gel, the nonuniform distributions of fiber volume fraction and the part height will be frozen up in the final part [Park et al. (2009)]. And this issue hasn't be studied in most of the previous related works. However, the compaction process has been studied in the consolidation of composite prepregs in autoclave forming process. Li et al. (2002, 2008) developed a numerical model to simulate the two-

dimensional flow and compaction process during the consolidation of laminated composites recently.

The purpose of the present work is to develop an efficient model for the resin flow across the compressible preform in RFI process. The two-dimensional resin flow is simulated by using the finite element method. In addition, the fabric preform is considered as deformable in the thickness direction. The resin pressure, the fiber volume fraction distribution, the infusion time and the height of final part can be investigated. To check the accuracy of the results, the numerical investigations are compared with those in Ref. [Park et al. (2009)]. Based on the simulation, people can determine the thickness of the resin film and preform to obtain the qualified products.

2 Mathematic model

2.1 Resin flow model

By ignoring the effects of the capillary, the porous flow of the resin through the deformable fabric preform can be described by the Darcy's law [Loos et al. (1996)] as follows

$$\phi \mathbf{v}_r = -\frac{\mathbf{K}}{\mu}\nabla P \tag{1}$$

where $\mathbf{K}$ is the permeability tensor for the fabric,P is the resin pressure, μ is the resin viscosity, ϕ is the volume fraction of fluid, and $\mathbf{v}_r$ is the relative velocity, i.e.,

$$\mathbf{v}_r = \mathbf{v}_l - \mathbf{v}_s \tag{2}$$

where $\mathbf{v}_s$ and $\mathbf{v}_l$ denote the fiber velocity and the resin velocity respectively. Since the parts made by RFI process are always thin enough, the resin gravity is ignored. Since the fabric preform is impregnated by the resin, it leads to

$$\phi + V_f = 1 \tag{3}$$

where V_f is the fiber volume fraction.

The continuity equations for the constant-density resin and the fiber can be written as

$$\text{resin: } \frac{\partial \phi}{\partial t} + \nabla \cdot (\phi \mathbf{v}_l) = 0 \tag{4}$$

$$\text{fiber: } \frac{\partial V_f}{\partial t} + \nabla \cdot (V_f \mathbf{v}_s) = 0 \tag{5}$$

Combining Eqs. (1)-(5), we can obtain the governing equation to describe the resin flow through a deformable porous medium [Park et al. (2003); Joubaud et al. (2005)] as

$$\nabla \cdot \left(\frac{\mathbf{K}}{\mu} \nabla P \right) = \nabla \cdot \mathbf{v}_s \tag{6}$$

or

$$\nabla \cdot \left(\frac{\mathbf{K}}{\mu} \nabla P \right) = -\frac{1}{V_f} \frac{\partial V_f}{\partial t} - \frac{1}{V_f} \mathbf{v}_s \cdot \nabla V_f \tag{7}$$

Eqs. (6) and (7) are equal because the terms on the right-hand side of them are equal by Eq. (5). Some researchers use Eq. (7) as the governing equation, and ignore the second term on the right-hand side of it by assuming that the resin flow and the fiber movement are sufficiently slow [Han et al. (2003); Park et al. (2009)]. The same assumption is also adopted in this work. The computing formulation of item $\nabla \cdot \mathbf{v}_s$ in Eq. (6) is discussed in subsection 2.2.

2.2 Fiber compaction effect

According to the Terzaghi's law [Terzaghi et al. (1967)], the effective stress σ_{eff} acting on the solid phase of a porous medium can be expressed as a function of the external stress P_c and the pore pressure P

$$\sigma_{eff} = P_c - P \tag{8}$$

Because the deformation in the transverse plane of the preform is much smaller than that in the thickness direction of the preform, and the volume strain of the resin is approach to zero, the terms on the right-hand side of Eq. (6) can be derived approximately as

$$\nabla \cdot \mathbf{v}_s = \frac{\partial}{\partial t} (\nabla \cdot \mathbf{u}_s) = \frac{\partial \varepsilon_v}{\partial t} = \frac{\partial \varepsilon_z}{\partial t} \tag{9}$$

where $\mathbf{u}_s$ is the displacement vector of the preform, ε_v is the volume strain of the fiber, and ε_z is the strain in the thickness direction of the preform. The stain ε_z can be expressed as a function of the thickness h as follows

$$\varepsilon_z = \frac{h - h_0}{h_0} \tag{10}$$

where h_0 is the initial height of the preform. Hence, the final form of Eq. (6) can be written as follows

$$\nabla \cdot \left(\frac{\mathbf{K}}{\mu} \nabla P \right) = \frac{\partial \varepsilon_z}{\partial t} \tag{11}$$

The permeability tensor $\mathbf{K}$ can be obtained through the experiments or the multi-scale analysis [Belov et al. (2004)]. The permeability of fabrics has been modeled in various mathematical expressions in terms of fiber volume fraction, such as the famous Kozeny-Carman equation [Park et al. (2003)]. In this study, we describe the permeability K as a function of the fiber volume fraction with a power-law model [Joubaud et al. (2005)]

$$K = a \cdot V_f^b \tag{12}$$

where parameters a and b can be obtained by the data fitting method with some experimental data.

The compressibility of fabrics has been studied by many authors [Robitaille et al. (1998); Gutowski et al. (1987)]. The compaction stress is expressed in terms of the fiber volume fraction usually. Similarly, we employ a power-law model to fit the experimental data [Park et al. (2009); Li et al. (2008)]

$$\sigma_{eff} = c \cdot V_f^d \tag{13}$$

where parameters c and d are experimental parameters depending on the fabric used.

Note that the fiber volume fraction can be expressed in terms of the thickness of the preform by the relation [Joubaud et al. (2005)]

$$V_f = \frac{NA_s}{h\rho_s} \tag{14}$$

where A_s is the superficial area density, i.e. , the weight of the reinforcement per unit area per layer, h is the thickness of the preform, N is the number of layers, and ρ_s is the density of fiber. Then NA_s/h is the density of the preform.

According to Eqs. (10) and (14), if we know the initial fiber volume fraction V_f^0, we can get the relation between ε_z and V_f

$$\varepsilon_z = \frac{V_f^0}{V_f} - 1 \tag{15}$$

As shown in Fig. 2, the permeability tensor $\mathbf{K}$ and the strain ε_z can be expressed by the resin pressure P.

Finally, we deduce the following governing equations from Eqs. (6)-(7)

$$\nabla \cdot \left(\frac{\mathbf{K}(P)}{\mu} \nabla P \right) = \frac{\partial \varepsilon_z(P)}{\partial t} \tag{16}$$

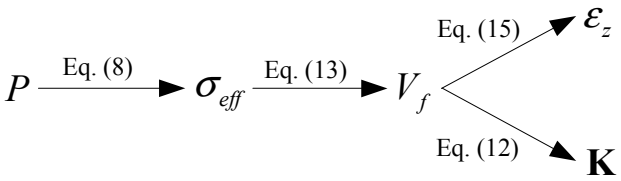

Figure 2: The relationship among variables.

or

$$\nabla \cdot \left(\frac{\mathbf{K}(P)}{\mu} \nabla P \right) = -\frac{1}{V_f(P)} \frac{\partial V_f(P)}{\partial t} \tag{17}$$

To solve the governing equations, we still need to describe the boundary and initial conditions, which are stated as follows

at the bottom of the preform: $P = P_c,\ V_f = V_f^0,\ \varepsilon_z = 0$ (18)

at the filling front or at the dry preform: $P = 0, V_f = V_f^c, \varepsilon_z = \varepsilon_z^c$ (19)

at the mold surface: $\dfrac{\mathbf{K}(P)}{\mu} \dfrac{\partial P}{\partial \mathbf{n}} = 0$ (20)

where P_c is the external pressure acting on the preform, V_f^c , ε_z^c are the fiber volume fraction and the strain under the external presssure P_c respectively, $\mathbf{n}$ is the direction normal to the mold surface. If the preform absorbed all the resin or the bleeder was saturated, we should use Eq. (20) to obtain the pressure boundary conditions at the bottom or at the top of the preform respectively. The numerical discrete formulations of above equations will be shown in Sec. 3.

3 Numerical methods

The finite element method and the finite difference method are used to discretize Eqs. (16)-(20) in this section. The volume of mould cavity is divided into a group of quadrilaterals, and we use the quadrilateral bilinear elements. In order to track the filling front, the unified VOF method [Mohan et al. (1999); Luoma et al. (2000)] is used. Here we select Eq. (16) for the discretized approximation. The pressure P and strain ε_z in the element e are discretized as follows

$$P|_e = \sum_{i=1}^{n_e} N_i P_i, \quad \varepsilon_z|_e = \sum_{i=1}^{n_e} N_i \varepsilon_z(P_i) \tag{21}$$

where N_i is the shape function at the node i of the element e, P_i is the nodal value of the pressure, n_e is the number of nodes in one element. Meanwhile we use the P^e for the calculation of the permeability tensor $\mathbf{K}$, which is the nodal value of resin pressure at the center of element e. Thus

$$P^e = \sum_{i=1}^{n_e} N_i(\mathbf{0}) P_i \tag{22}$$

Using the Galerkin-weighted residual formulation on Eq. (16), we obtain

$$\begin{aligned} &\sum_e \sum_{i=1}^{n_e} \left[\frac{\partial}{\partial t} \int_{\Omega^e} N_i \varepsilon_z(P_i) N_j d\Omega^e \right] = \sum_e \int_{\partial\Omega^e} \left(\frac{\mathbf{K}(P^e)}{\mu} \nabla P \cdot \mathbf{n} \right) N_j d\partial\Omega^e \\ &- \sum_e \sum_{i=1}^{n_e} \left[\int_{\Omega^e} \nabla N_i^T P_i \frac{\mathbf{K}(P^e)}{\mu} \nabla N_j d\Omega^e \right] \quad j = 1, 2 \cdots n_e \end{aligned} \tag{23}$$

where Ω^e and $\partial\Omega^e$ are the discrete domain and the boundary of the element e respectively. Eq. (23) can be written as

$$\mathbf{C}\dot{\varepsilon}_z(\mathbf{P}) + \mathbf{M}(\mathbf{P})\mathbf{P} = \mathbf{f} \tag{24}$$

where

$$\mathbf{C} = \sum_e TEG \left(\int_{\Omega^e} \mathbf{N}^T \mathbf{N} d\Omega^e \right) \tag{25}$$

$$\mathbf{M}(\mathbf{P}) = \sum_e TEG \left(\int_{\Omega^e} \nabla \mathbf{N}^T \frac{\mathbf{K}(P^e)}{\mu} \nabla \mathbf{N} d\Omega^e \right) \tag{26}$$

$$\mathbf{f} = \sum_e TEG \left(\int_{\partial\Omega^e} \left(\frac{\mathbf{K}(P^e)}{\mu} \nabla P \cdot \mathbf{n} \right) \mathbf{N} d\partial\Omega^e \right) \tag{27}$$

and

$$\mathbf{N} = (N_1, N_2 \cdots N_{n_e}) \tag{28}$$

where *TEG* is the global assembling operator. Introducing the finite difference approximation for the time derivative term in Eq. (12), we obtain

$$\dot{\boldsymbol{\varepsilon}}_z(\mathbf{P}) = \frac{\boldsymbol{\varepsilon}_z^{n+1}(\mathbf{P}) - \boldsymbol{\varepsilon}_z^n(\mathbf{P})}{\Delta t} \tag{29}$$

Then the discretized governing equation is given by

$$\mathbf{C}\left[\boldsymbol{\varepsilon}_z^{n+1}(\mathbf{P}) - \boldsymbol{\varepsilon}_z^n(\mathbf{P})\right] + \Delta t \mathbf{M}(\mathbf{P})\mathbf{P} = \Delta t \mathbf{f} \tag{30}$$

The resin pressure field can be got by solving Eq. (30). The calculated pressure is then used to update the fill factors in the VOF method for tracking the filling front. In order to solve the nonlinear partial differential equation, the Newton iterative method is used. The iterative algorithm is presented in Fig. 3.

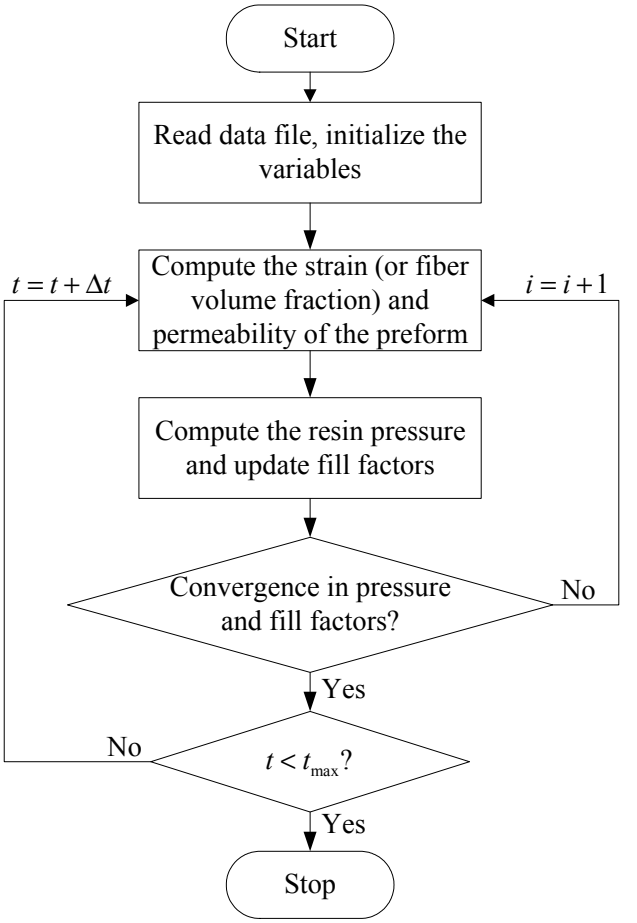

Figure 3: Proposed algorithm for the RFI modeling.

4 Simulation results

In order to check the accuracy of the presented numerical scheme, a simple rectangular geometry has been selected to compare the simulated results and the analytical solutions got by Park et al. (2009). Then we perform a parametric study

to investigate the influences of the initial resin film thickness on the final thickness of the part and on the fiber volume fraction distribution. Finally, the effects of the external pressure and the amount of the bleeder on the final thickness of the part and on the resin pressure distribution are also studied.

4.1 Validation of the numerical model

The material parameters used here are listed in Ref. [Park et al. (2009)]. The viscosity of the resin is 1 *Pa s* for approximation. Actually, the viscosity is a time-dependent variable since the resin has thermo-chemical reaction [Lee et al. (1982)]. The schematic of the resin infusion process is presented in Fig. 4.

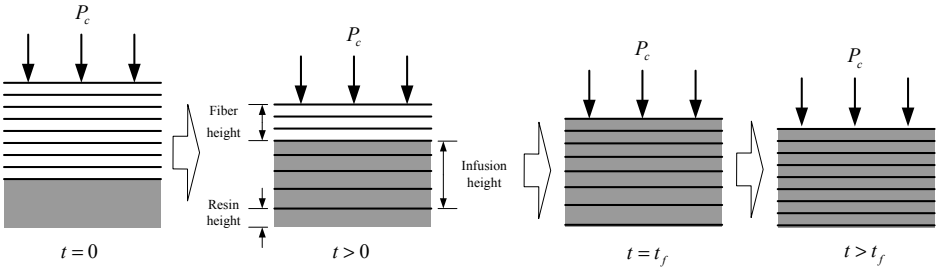

Figure 4: Schematic diagram of the resin flow and the fiber compaction during RFI process.

We choose the same conditions as those in the case b in Ref. [Park et al. (2009)] for the simulation. A good agreement between the two profiles can be observed by Fig. 5. However, the resin infusion heights are not fitted well at the beginning. This may be caused by the accuracy of the numerical simulation, such as the limit of grids, time steps and the accuracy of the VOF method. The resin infusion time is 696*s*, and it's 738*s* in Ref. [Park et al. (2009)].

The external pressure is carried by resin and the fiber during the resin infusion process. Therefore, the resin pressure leads to the swelling of the preform when the resin impregnates the preform. It's shown clearly in Fig. 6, where the mesh denotes the initial shape of the preform. Meanwhile, the fiber volume fraction distribution is nonuniform in the thickness direction of the preform.

4.2 Model application in the infusion and compaction process

In the numerical experiment, the quasi-steady state assumption and the updated Lagrange formulation are implemented [Celle et al. (2008); Li et al. (2008)]. The permeability and compressibility model parameters for G0814 carbon fiber weave are

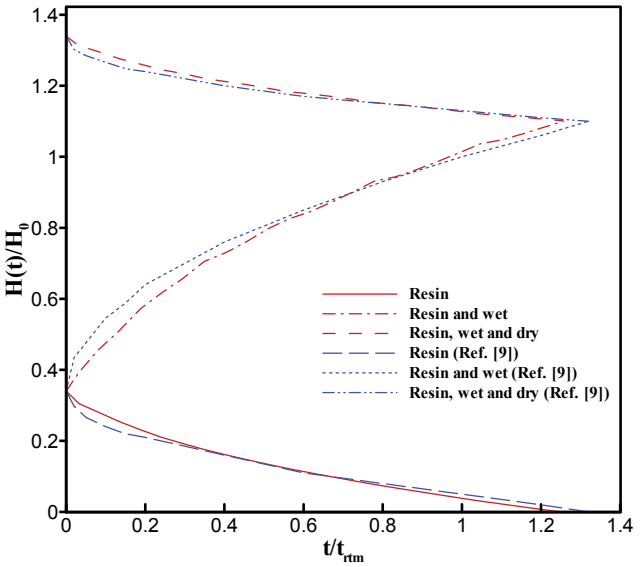

Figure 5: Evolutions of the thicknesses of resin film, the resin infused fabric and the dry fabric.

Tab. 1 Parameters of preform permeability and compressibility

$K_x = a \cdot V_f^b$	a=1.167×10^{-14}
	b=−8.473
$K_z = a' \cdot V_f^{b'}$	a'=5.873×10^{-16}
	b'=−8.071
$\sigma_{eff} = c \cdot V_f^d$	c=4.896×10^8
	d=9.632

listed in Tab. 1. The variation of the resin viscosity for 5405 BMI (Bismaleimide) resin is shown in Fig. 7. And the mold temperature for resin infusion is 130°.

It's important to estimate the resin infusion time and the resin film thickness required to fully impregnate a fabric preform. So we perform three cases to investigate the effects of the different initial resin film thickness (Tab. 2). The external

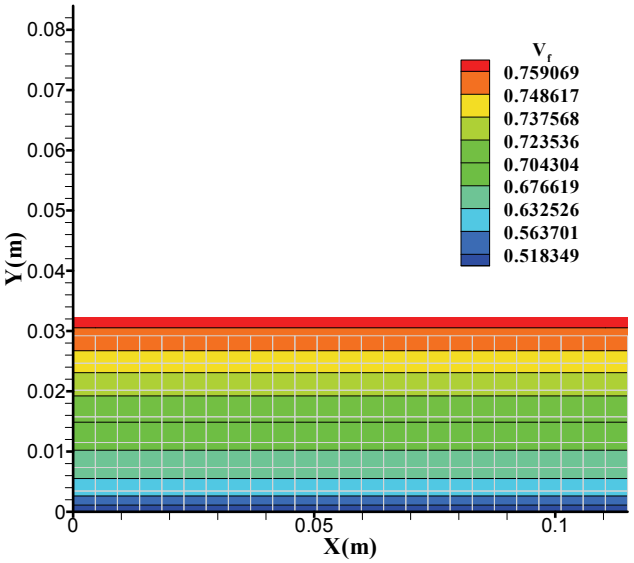

Figure 6: The fiber volume fraction distribution.

Tab. 2 The resin infusion time and the part heights in different cases.

Cases	Initial thickness of resin film	Resin infusion time	Part height at 34min
a	21*mm*	336*s*	32.41*mm*
b	30*mm*	336*s*	32.64*mm*
c	17*mm*	225*s*	32.26*mm*

pressure is fixed to 0.4*MPa*, and the initial thickness of dry fabric under external pressure is fixed to 32.25*mm*. The bleeder is considered to absorb all the extra resin here.

As described in case b in Fig. 8, the resin film is excessive. When the extra resin flows into the bleeder, the potential residual voids [Celle et al. (2008)] can be decreased. On the contrary, if the resin film is not much enough, it still can impregnate

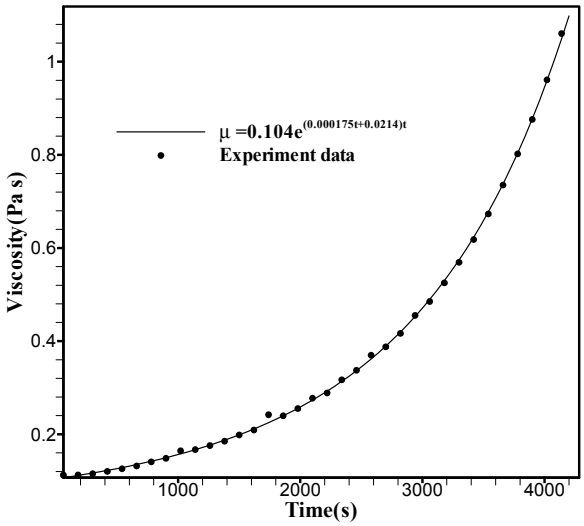

Figure 7: The viscosity curve of BMI resin in 130˚C.

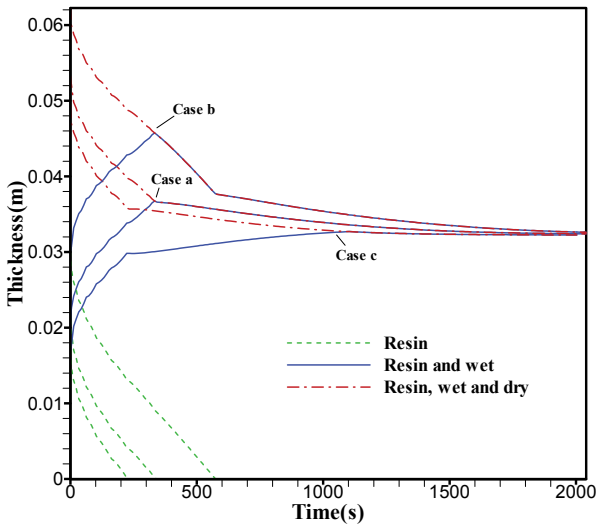

Figure 8: Evolutions of the thicknesses of resin film, the resin infused fabric and the dry fabric in three cases.

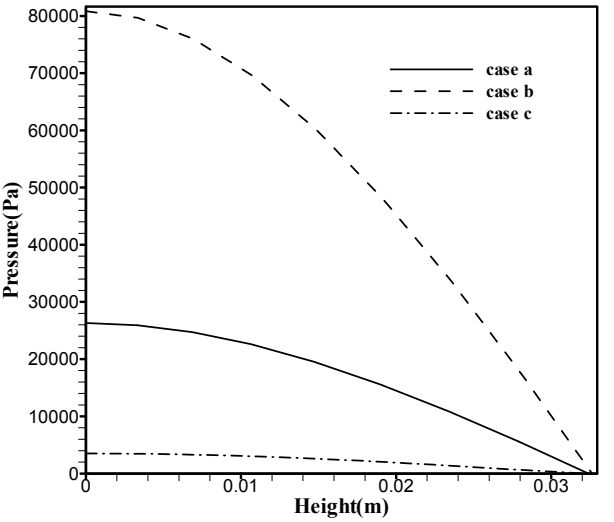

Figure 9: Resin pressure distributions in the thickness direction at 34min.

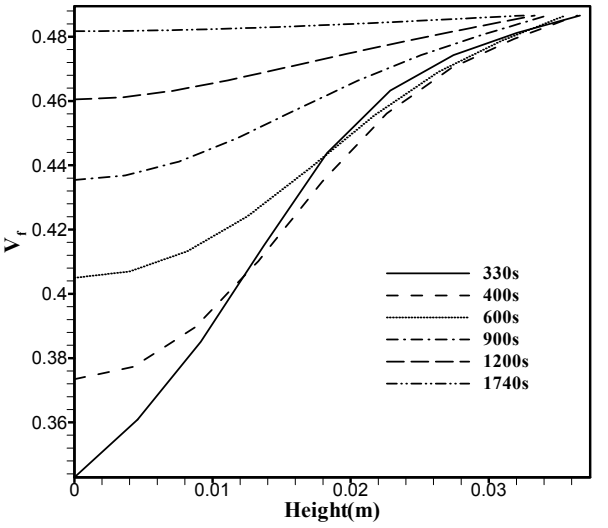

Figure 10: Fiber volume fraction distributions in the thickness direction at different time in case

Tab. 3 The material parameters and the external pressure profile.

Resin film thickness	30 *mm*
Preform thickness under 0.1 *MPa*	33.00 *mm*
The amount of resin (thickness) can be absorbed by bleeder	16.17 *mm*
External pressure profile	$0.1MPa \xrightarrow{\text{after } 521s} 0.3MPa \xrightarrow{\text{after } 600s} 0.6MPa$

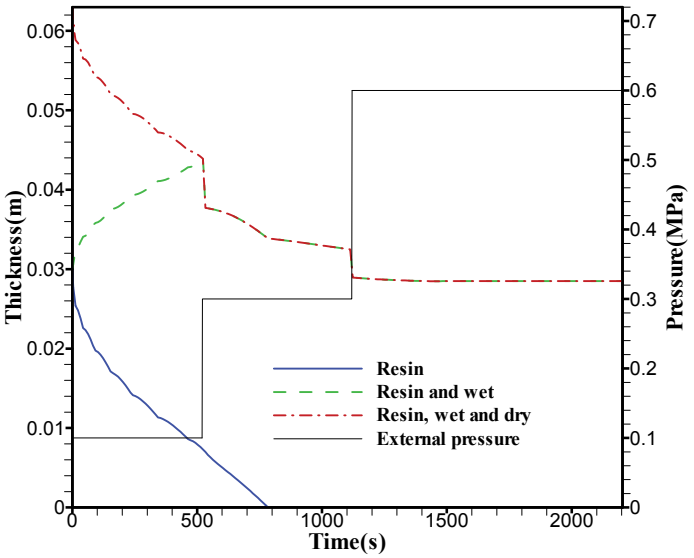

Figure 11: Evolutions of the thicknesses of resin film, the resin infused fabric and the dry fabric under the external pressure profile.

the preform fully under the compact pressure in some situations (case c in Fig. 8). Based on the Fig. 8, one can observe the evolution of the resin film thickness, the resin infusion height and the preform height easily.

Of all the cases shown in Fig. 9, the resin pressure distribution is the lowest in case c. It results in the lowest final thickness of the part (Tab. 2). Before the preform is impregnated, the fiber and the resin carry the external pressure together in the im-

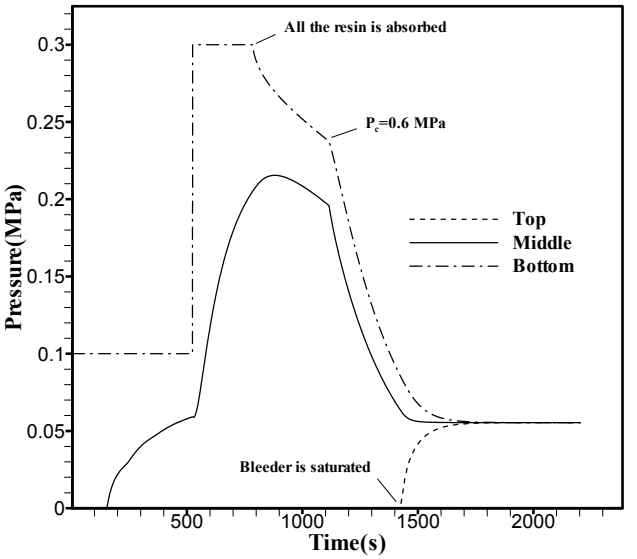

Figure 12: Evolutions of the resin pressure in the different positions of the preform.

pregnated region, while the fiber carries the external pressure in the unfilled region. After the preform is fully impregnated, the fiber carries more stress since the resin pressure drops. Hence, the fiber stress and the fiber volume fraction distribution will become uniformer in the thickness direction of the preform (Fig. 10).

According to the previous analysis, one can choose the right thickness of the resin film and the external pressure to eliminate the unfilled region and to get the proposed height of the part.

4.3 Model application for the optimization

During the resin infusion process, many factors such as the external pressure and the bleeder thickness can affect the quality of the product. So a parametric study for the optimization is presented here.

To reduce the air voids, the resin must have suitable velocity [Trochu et al. (2006); Leclerc et al. (2008)] and pressure [Sevostianov et al. (2000); Campbell (2004)]. If the void pressure exceeds the resin pressure, the void growth will potentially occur. Overbleeding can cause a large drop in resin pressure as proposed in Ref. [Campbell et al. (2006)]. Based on the previous results, the resin pressure will

drop when all the resin is absorbed by the preform and the bleeder. However, when the bleeder is saturated, the resin can't flow into it, and the resin pressure will stop dropping. Thus, we can select the suitable amount of the bleeder to keep the resin pressure constant after the bleeder is saturated. The parameters of the material and the external pressure profile are shown in Tab. 3.

Shown in Fig. 11 is the evolution of the resin film thickness, the resin infusion height and the preform height under the given pressure profile. At the beginning of the resin infusion process stage, the low external pressure can make the resin to flow slowly for avoiding the macro-voids. When the fabric is filled fully at $521s$, a higher external pressure is introduced for the compaction of the preform. The external pressure is raised to $0.6MPa$ at $1121s$ to ensure the proposed height of the final part and the fiber volume fraction. When all the resin is absorbed, the resin pressures begin to drop. And when the bleeder is saturated, the resin pressures in the different positions of the preform are convergence to the same value (Fig. 12).

According to the above simulation, if we choose the suitable amount of the bleeder, we can keep the resin pressures being the required value in the end. Finally, we can reduce the void content, and get the optimized part with the proposed thickness and the fiber volume fraction.

5 Conclusions

In this work, a numerical modeling of the resin flow and the fiber compaction has been carried out for the RFI process. The finite element method was used to simulate the process, and the VOF method was used to track the filling front. The resin pressure, the fiber volume fraction distribution, resin infusion time and the part height were obtained.

The accuracy of the numerical model was verified by comparing the numerical results with the analytical results, and a good agreement was observed. By using this model, a parametric study about the effects of the resin film thickness and the optimizing conditions was performed. The model can be used to estimate the quality of the product or to optimize the processing conditions such as the external pressure.

Acknowledgement: The authors would like to acknowledge Prof. Chen Lixin's research group for the kindness to provide us the experiment data. The work was supported by National Natural Science Foundation of China (No: 90916027–11071196) and the Scientific Research Foundation for the Returned Overseas Chinese Scholars (No: 2009YK11).

References

Belov, E.B.; Lomov, S.V.; Verpoest, I.; Peters, T.; Roose, D.; Parnas, R.S.; Hoes, K.; Sol, H. (2004): Modelling of permeability of textile reinforcements: lattice Boltzmann method, *Composite Science and Technology*, vol.64, no.7-8, pp. 1069-1080

Campbell, F.C. (2004): Manufacturing processes for advanced composites, *Elsevier*

Campbell, F.C.; Mallow, A.R.; Browning, C.E. (1995): Porosity in carbon fiber composites: an overview of cause, *Journal of Advanced Materials*, vol.26, no.4, pp. 18-33

Celle, P.; Drapier, S.;, Bergheau, J.M. (2008): Numerical modelling of liquid infusion into fibrous media undergoing compaction, *European Journal of Mechanics-A/Solids*, vol.27,no.4, pp. 647-661

Govignon, Q.; bickerton, S.; Kelly, P.A. (2010): Simulation of the reinforcement compaction and resin flow during the complete resin infusion process, *Composites Part A: Applied Science and Manufacturing*, vol.41, no.1, pp. 45-57

Gutowski, T.G.; Morigaki, T.; Cai, Z. (1987): The consolidation of laminate composites, *Journal of Composite Materials*, vol.21, no.2, pp. 172-188

Han, N.L.; Suh, S.S.; Yang, J-M.; Hahn H.T. (2003): Resin film infusion of stitched stiffened composite panels, *Composites Part A: Applied Science and Manufacturing*, vol.34, no.3, pp. 227-236

Joubaud, L.; Achim, V.; Trochu, F. (2005): Numerical simulation of resin infusion and reinforcement consolidation under flexible cover, *Polymer Composites*, vol. 26, no.4, pp. 417-427

Leclerc, J.S.; Ruiz, E. (2008): Porosity reduction using optimized flow velocity in Resin Transfer Molding, *Composites Part A: Applied Science and Manufacturing*, vol.39, no.12, pp. 1547-1568

Lee, W.I.; Loos, A.C.; Springer, G.S. (1982): Heat of reaction, degree of cure, and viscosity of hercules 3501-6 Resin, *Journal of Composite Materials*, vol.16, no.6, pp. 510-520

Li, M.; Li, Y.; Zhang, Z.; Gu, Y. (2008): Numerical simulation of two dimensional flow and compaction during the consolidation of laminated composites, *Polymer Composites*, vol.29, no.5, pp. 560-568

Li, M.; Tucker ?, C.L. (2002): Modeling and simulation of two-dimensional consolidation for thermoset matrix composite, *Composites Part A: Applied Science and Manufacturing*, vol.33, no.6, pp. 877-892

Li. J.; Zhang, C.; Liang, R.; Wang, B.; Walsh, S. (2008): Modeling and analysis of thickness gradient and variations in vacuum-assisted resin transfer molding process, *Polymer Composites*, vol.29, no.5, pp. 473-482

Loos, A.C.; MacRae J.D. (1996): A process simulation model for the manufacture of a blade-stiffened panel by the resin film infusion process, *Composites Science and Technology*, vol.56, no.3, pp. 273-289

Luoma, J.A.; Voller, V.R. (2000): A explicit scheme for tracking the filling front during polymer mold filling, *Applied Mathematical Modelling*, vol.24, no.8-9, pp. 575-590

Mohan, R.V.; Ngo, N.D.; Tamma, K.K. (1999): On a pure finite-element-based methodology for resin transfer molds filling simulations, *Polymer Engineering and Science*, vol.39, no.1, pp. 26-43

Ouahbi, T.; Saouab, A.; Bréard, J.; Ouagne, P.; Chatel, S. (2007): Modelling of hydro-mechanical coupling in infusion process, *Composites Part A: Applied Science and Manufacturing*, vol.38, no.7, pp. 1646-1654

Park, C.H.; Saouab, A. (2009): Analytical modeling of composite molding by resin infusion with flexible tooling: VARI and RFI process, *Journal of Composite Materials*, vol.43, no.18, pp. 1877-1900

Park, J.; Kang, M.K. (2003): A numerical simulation of the resin film infusion process, *Composite Structure*, vol.60, no.4, pp. 431-437

Robitaille, F.; Gauvin, R. (1998): Compaction of textile reinforcements for composites manufacturing ?: Compaction and relaxation of dry and H_2O-Saturated woven reinforcements, *Polymer Compisites*, vol.19, no.5, pp. 543-557

Sevostianov, I.; Verijenko, V.E.; von Klemperer, C.J. (2000): Mathematical model of cavitation during resin film infusion process, *Composite Structures*, vol.48, no.1-3, pp. 197-203

Shojaei, A. (2006): Numerical simulation of three-dimensional flow and analysis of filling process in compression resin transfer moulding, *Composites Part A: Applied Science and Manufacturing*, vol.37, no.9, pp. 1434-1450

Shojaei, A. (2006): A numerical study of filling process through multilayer preforms in resin injection/compression molding, *Composites Science and Technology*, vol.6, no.11-12, pp. 1546-1557

Terzaghi, K.; Peck, R.; Mesri, G. (1967): Soil mechanics in engineering practice, *Jones Wiley & Sons*

Trochu, F.; Ruiz, E.; Achim, V.; Soukane, S. (2006): Advanced numerical simulation of liquid composite molding for process analysis and optimization, *Composites Part A: Applied Science and Manufacturing*, vol.37, no.6, pp. 890-902